Hindawi Publishing Corporation
Journal of Nanotechnology
Volume 2011, Article ID 386503, 8 pages
doi:10.1155/2011/386503

*Research Article*

# Light-Emitting Polymer Nanocomposites

**Kyle Gipson, Brett Ellerbrock, Kathryn Stevens, Phil Brown, and John Ballato**

*Center for Optical Materials Science and Engineering Technologies (COMSET) and The School of Materials Science and Engineering, Clemson University, Clemson, SC 29634, USA*

Correspondence should be addressed to John Ballato, jballat@clemson.edu

Received 15 March 2011; Accepted 28 April 2011

Academic Editor: Hongmei Luo



Inorganic nanoparticles doped with optically active rare-earth ions and coated with organic ligands were synthesized in order to create fluorescent polymethyl methacrylate (PMMA) nanocomposites. Two different aromatic ligands (acetylsalicylic acid, ASA and 2-picolinic acid, PA) were utilized in order to functionalize the surface of $Tb^{3+}:LaF_3$ nanocrystals. The selected aromatic ligand systems were characterized using infrared spectroscopy, thermal analysis, rheological measurements, and optical spectroscopy. Nanoparticles produced *in situ* with the PMMA contained on average 10 wt% loading of $Tb^{3+}:LaF_3$ at a 6 : 1 La : Tb molar ratio and ~7 wt% loading of 4 : 1 La : Tb molar ratio for the PA and ASA systems, respectively. Measured diameters ranged from $457 \pm 176$ nm to $150 \pm 105$ nm which is indicative that agglomerates formed during the synthesis process. Both nanocomposites exhibited the characteristic $Tb^{3+}$ emission peaks upon direct ion excitation (350 nm) and ligand excitation (PA : 265 nm and ASA : 275 nm).

## 1. Introduction

Rare-earth (RE) ions doped into inorganic matrices have been utilized as luminescent additives in applications such as light-emitting devices, lasers, optical amplifiers, and biological fluorescence labeling [1]. RE ions are ideal additives due to their ability to produce intense narrow spectral bands in the visible range of the electromagnetic spectrum and exhibit long excited-state lifetimes as a result of f-f electronic transitions [2, 3].

With respect to many inorganic materials, polymer matrices have the potential to offer improved production rates, lower cost, and improved processability. However, polymers exhibit inherently high vibrational energies which tend to quench many of the transitions of rare-earth ions thus limiting their application as optical materials [4]. RE ions are typically incompatible with organic polymers; although, PMMA has been shown suitable when utilized as a matrix for certain RE ion ligand complexes [5].

In this research, the method utilized to overcome high vibrational energy observed in PMMA is to incorporate optically active RE ions into low vibrational energy inorganic nanoparticles which then are dispersed into a polymer matrix by the use of selective organic ligands. The inorganic component is rare-earth ion phosphor, (terbium III), doped lanthanum trifluoride ($LaF_3$) nanocrystals. Terbium (III) ($Tb^{3+}$) emits green fluorescence as a result of a strong electronic transition, $^5D_4 \rightarrow {}^7F_5$, occurring near 543 nm. $Tb^{3+}$ exhibits absorption levels at shorter wavelengths in the ultraviolet (UV) to visible color region (390–780 nm) [6]. Consequently, RE ions like $Tb^{3+}$ are incorporated into an inorganic host that is surface-treated or capped with UV light harvesting ligands to boost the absorption capability of the RE.

$Tb^{3+}$ is incorporated into the inorganic crystal structure of lanthanum trifluoride, $LaF_3$ to create the doped nanocrystal ($Tb^{3+}:LaF_3$). $LaF_3$, was chosen as the host matrix for terbium due to the low phonon energy it exhibits which minimizes the quenching potential of $Tb^{3+}$ ion emissions [7–10]. The organic portion refers to UV light harvesting ligands that bind to the surface of the nanocrystal to form a coordination complex. The ligands purpose is to enhance emissions and aid in dispersion within the organic polymer matrix. Light harvesting refers to the ability of the ligand to absorb light from short wavelengths and transfer the energy to the rare-earth ion which emits light at longer wavelengths [3, 11]. The light-harvesting ligand capped nanocrystal complex is considered to be the complete nanoparticle.

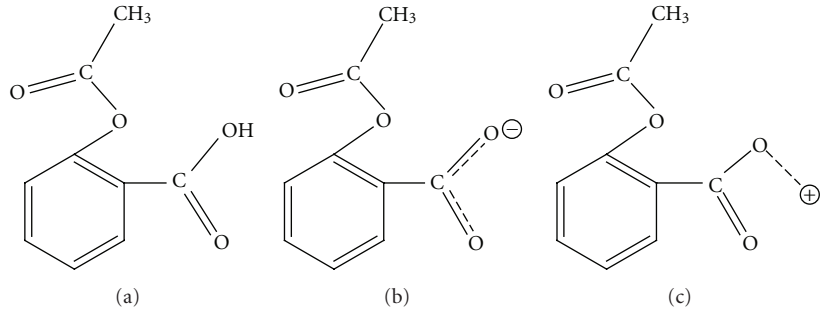


Figure 1: ASA molecule (a), ASA anion (b), and ASA chelation of cation (c).

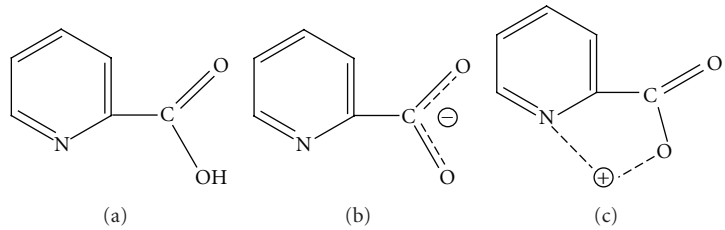


Figure 2: PA molecule (a), PA anion (b), and PA chelation of cation (c).

Aromatic acids have been used as ligands to sensitize and enhance lanthanide fluorescence by reducing the probability of radiationless (heat) energy transfer from the RE ion to the solvent [12]. Both acetylsalicylic acid (ASA) and 2-picolinic acid (PA) are aromatic acids and bidentate ligands. ASA deprotonates the carboxyl group which forms dianions with the ability to coordinate cations like RE ions [13]. The structures of ASA are depicted in Figure 1: (a) molecule, (b) anion where the hydrogen of carboxyl group was ionized, and (c) chelated structure of cation where the oxygen of the carboxyl group bonds to the cation. PA chelates cations through the nitrogen atom of the pyridine ring and the oxygen anion of deprotonated carboxyl group as illustrated in Figure 2. In Figure 2, (a) is the molecule, (b) is the anion where the hydrogen of carboxyl group was ionized, and (c) is the chelated structure of cation where the oxygen of the carboxyl group acts with the nitrogen atom to bond with the cation [14].

The incorporation and distribution of nanoparticles has been shown to affect the viscoelastic properties of polymers [15]. The focus of this research is to develop light-emitting polymer nanocomposites via solution/precipitation chemistry in order to understand the influence of the nanoparticles on the thermal, rheological, and photoluminescence characteristics of the resultant polymer nanocomposite.

## 2. Experimental

*2.1. Materials.* The PMMA ($M_w \approx 130$ k—Plaskolite West, Inc.) was used as received. Anhydrous tetrahydrofuran, THF (99%—Acros), methanol (99.8%—BDH), and ultrapure water (18.2 MΩ·cm) were used as solvents. Lanthanum (III) nitrate hexahydrate, La ($La(NO_3)_3 \cdot 6H_2O$, 99.99%—Sigma-Aldrich) and terbium (III) nitrate hydrate, $Tb^{3+}$ ($Tb(NO_3)_3 \cdot 6H_2O$, 99.9%—Sigma-Aldrich), acetylsalicylic acid, ASA (MP Biomedicals, LLC), 2-picolinic acid, PA (99%—Alfa Aesar), ammonium fluoride (99.3%—Fisher Scientific), ammonium hydroxide (28–30% ACS—BDH Aristar-VWR), ethanol-EtOH (99.5%—Acros), and acetone (99.9%—BDH) were used as received.

*2.2. Synthesis.* The nanoparticles were produced by the scheme shown in Figure 3.

*2.3. Characterization.* Dried precipitated polymer and precipitated polymer nanocomposite samples were analyzed by attenuated total reflectance—Fourier transform infrared (ATR-FTIR) spectroscopy. The spectra were acquired on a Theromo-Fisher Nicolet Magna 550 FTIR spectrometer equipped with a Thermo-SpectraTech Foundation Series Diamond ATR accessory, Nic-Plan microscope, and Omnic software. The spectral resolution was set at 8 $cm^{-1}$ and 160 scans were conducted at room temperature.

Glass transition temperature ($T_g$) was determined by a Universal TA Instruments—2920 MDSC V2.6A differential scanning calorimeter (DSC). Approximately 5 mg of sample was placed in a hermetic sample pan for measurements. The instrument was equilibrated at a temperature of 25°C. The temperature ramp rate was set at 20°C/min to a maximum of 300°C. The samples were removed, quenched with liquid nitrogen, and then rerun under the same heating regimen. The traces were analyzed using TA Instruments Universal Analysis 2000 version 4.4a software.

Percent nanocrystal loading was determined by a Universal TA Instruments—TGA Q5000 V3.5 Build 252 thermogravimetric analysis instrument (TGA). Samples weighing

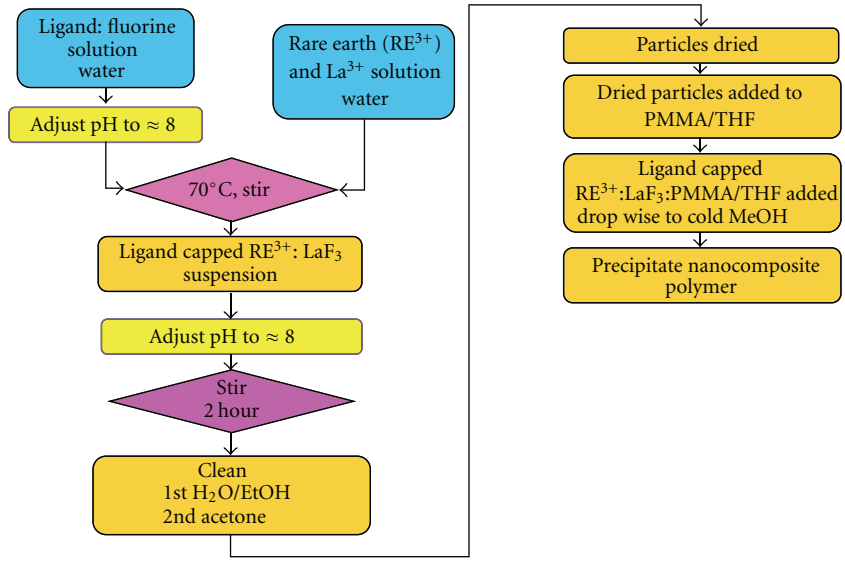


Figure 3: Flow chart of nanoparticle synthesis.

approximately 5 mg were loaded into a platinum pan and then placed in the instrument under nitrogen. The temperature ramp rate was 10°C/min to 650°C. Nanoparticle loading values were determined from the percent of material remaining at 495°C using TA Instruments Universal Analysis 2000 version 4.4a software.

Size and size distribution of particles were measured on a Malvern Dynamic Light Scattering (DLS) Zetasizer Nano Series Nano ZS at room temperature. Teflon spheres were used to ball-mill the dried samples into a fine powder before a resuspension in a neat solvent. The average of three samples was used to determine the size and size distributions.

Viscosity measurements were performed using a TA Instruments—ARES LS/M 0012701 Rheometer equipped with the TA Orchestrator version 7.1.2.3 software package. Dynamic frequency sweep tests were performed under a nitrogen environment in the frequency range of 0.1 to 500 rad/s at 220°C. Cone and plate geometry was used where the plates had a diameter of 25 mm and the cone angle was set at 0.1 rad. The gap distance during the measurements was set at 0.056 mm and the strain was maintained at 5%.

A Perkin Elmer Lambda 900 UV-Vis-NIR Spectrometer with UV Winlab Version 3.00.03 software was utilized to gather optical absorption data. Scans were performed with a 1 nm slit size in the UV and visible range of 260–380 nm. Samples were prepared by dispersing the ligand into water and measurements were done at room temperature.

Photoluminescence measurements were performed with a Jobin-Yvon Fluorolog Tau 3 Fluorometer with 4 nm emission bandpass. The data were collected at 1 nm intervals with 50 ms integration time. All measurements were performed at room temperature. Excitation spectra were fit with Lorentzian curves correcting for a constant background in Igor Pro 6.1 (Wavemetrics, Portland, Oregon) for full width at half maximum (FWHM) measurements.

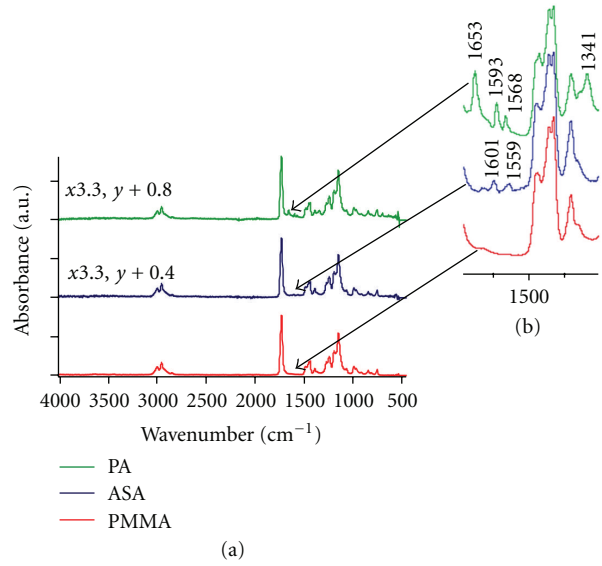


Figure 4: Absorbance as a function of wavenumber—infrared spectra of undoped precipitated PMMA (red), ASA capped nanocrystals incorporated into precipitated PMMA (blue), and PA capped nanocrystals incorporated into precipitated PMMA (green) in the range of 4000–500 $cm^{-1}$ (a) and inset—range 1700–1300 $cm^{-1}$ (b).

## 3. Results and Discussion

*3.1. Characterization of Ligand Capped Nanoparticles.* Figure 4 shows the FT-IR spectra comparison of undoped precipitated PMMA, ASA and PA capped nanocrystals loaded into PMMA. The region of interest is located in the range of 1700–1300 $cm^{-1}$, inset of Figure 4. Absorption peaks at 1601 $cm^{-1}$ and 1559 $cm^{-1}$ were observed in FT-IR spectrum for the ASA, doped PMMA and suggest benzene ring stretching. The spectrum for the PA doped system exhibits absorption peaks at around 1653 $cm^{-1}$, 1593 $cm^{-1}$,

Table 1: Percent loadings and glass transition temperature of ligand capped nanocrystals in PMMA.

| Ligand | Ligand to nanoparticle ratio | Calculated loading | Experimental loading | Inflection point $T_g$, °C |
|---|---|---|---|---|
| ASA | 2 : 1 | 10% | 9% | 120 |
| | 3 : 1 | 10% | 9% | 121 |
| | 4 : 1 | 10% | 10% | 121 |
| | 5 : 1 | 10% | 10% | 121 |
| PA | 2 : 1 | 10% | 7% | 121 |
| | 3 : 1 | 10% | 7% | 122 |
| | 4 : 1 | 10% | 7% | 120 |
| | 5 : 1 | 10% | 8% | 121 |
| undoped PMMA precipitated | | | 0% | 122 |

Table 2: Elemental composition and corresponding atomic percentage of nanoparticles in PMMA at different ligand:nanoparticle ratios.

| | Atomic percentage | | | | | | | |
|---|---|---|---|---|---|---|---|---|
| | PA | | | | ASA | | | |
| Element | 2 : 1 | 3 : 1 | 4 : 1 | 5 : 1 | 2 : 1 | 3 : 1 | 4 : 1 | 5 : 1 |
| La | 61.2 | 46.4 | 49.1 | 30.8 | 43.0 | 30.4 | 32.6 | 30.8 |
| Tb | 6.6 | 8.0 | 8.1 | 4.9 | 9.1 | 8.2 | 7.7 | 7.3 |
| F | 32.2 | 45.6 | 42.7 | 64.3 | 47.9 | 61.4 | 59.5 | 60.0 |

and 1568 $cm^{-1}$ which can be associated with aromatic ring stretching of the pyridine ring of picolinic acid. The IR peak observed at approximately 1341 $cm^{-1}$ could correspond to the C-N stretching vibrations of the PA ligand. Therefore, both ligands are present in the PMMA matrix.

The loading of the inorganic components ($Tb^{3+}$ : $LaF_3$) and $T_g$ obtained from TGA and DSC, respectively, are presented in Table 1. PMMA loaded with ASA ligand capped nanoparticles (hence forth referred to as the ASA system) contained ~10 wt% inorganic material. Whereas the PMMA loaded with PA ligand capped nanoparticles (PA system) contained inorganic material on the order of 7 wt%. However, the measured amounts of inorganic material for each ligand sample were kept constant experimentally. The difference in inorganic material amounts might be attributed to loss of product during the cleaning steps of the particle synthesis.

No significant change in $T_g$ was observed between the undoped PMMA and the nanoparticle-loaded PMMA systems. The glass transition inflection point was used to determine the $T_g$ and the average of two sample runs is stated as the $T_g$ for each sample in Table 1.

The results of the elemental composition of the nanoparticles determined by EDS analysis are summarized in Table 2. This data confirms that the resulting nanoparticles consisted of $Tb^{3+}$ : $LaF_3$ at a 6 : 1 and 4 : 1 (La : Tb) molar ratio for the PA and ASA systems, respectively.

Suspensions containing different ligand : nanoparticle ratios of PA : $Tb^{3+}$ : $LaF_3$ and ASA : $Tb^{3+}$: $LaF_3$ were measured by dynamic light scattering to determine the size of the nanoparticles. Previous work of Ellerbrock using the same nanoparticle synthesis route found that $Tb^{3+}$ : $LaF_3$ particles without ligand measured 6 ± 1 nm in diameter [16]. The average diameter for PA : $Tb^{3+}$ : $LaF_3$ and ASA : $Tb^{3+}$: $LaF_3$ are presented in Table 3. The large diameters produced suggest that particulate agglomerates formed. Figure 5 shows a representative illustration of agglomerates ranging from 50–1000 nm within the nanocomposite. Due to the measured agglomerate diameters being on the order of the excitation wavelength of the rare-earth ion (~350 nm), the light is scattered resulting in reduced light emission. Additionally, synthesis parameters have been suggested as the cause of agglomerate formation as they can cause changes in the electrostatic nature of nanoparticles in solutions [17].

Table 3: Agglomerate diameters and complex viscosity percent difference of ligand capped nanocrystals in PMMA.

| Ligand | Ligand to nanoparticle ratio | Diameter (nm) | Complex viscosity percent difference |
|---|---|---|---|
| ASA | 2 : 1 | 252 ± 66 | 81% |
| | 3 : 1 | 420 ± 116 | 66% |
| | 4 : 1 | 349 ± 85 | 58% |
| | 5 : 1 | 233 ± 41 | 68% |
| PA | 2 : 1 | 444 ± 138 | 44% |
| | 3 : 1 | 150 ± 105 | 82% |
| | 4 : 1 | 457 ± 176 | 53% |
| | 5 : 1 | 242 ± 24 | 70% |

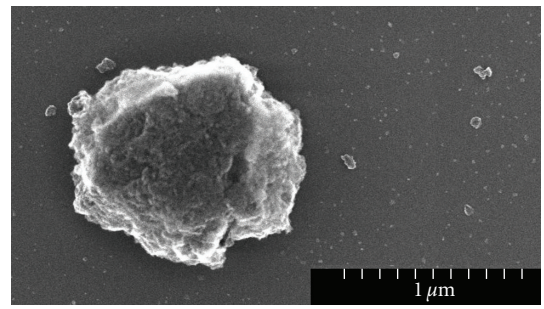


Figure 5: STEM image of polymer nanocomposite showing the presence of 50–1000 nm ligand capped $Tb^{3+}$ : $LaF_3$ agglomerates.

No significant difference was observed between the size of the agglomerates resuspended in water versus those resuspended in THF for either PA or ASA ligand at nanoparticle ratios of 2 : 1, 3 : 1, and 4 : 1. However, a significant particle size difference was observed at the 5 : 1 ratio between the two resuspension methods. The agglomerate sizes in water for ASA and PA systems were measured at 893 ± 418 nm and 1080 ± 192 nm, respectively. The agglomerate sizes in THF/PMMA were measured at 233 ± 41 nm for ASA and 242 ± 24 nm for PA. This diameter variation could be attributed to the mechanical action of the grinding process necessary to achieve the resuspension. Representative histograms of the diameter size distribution for PA : $Tb^{3+}$ : $LaF_3$ and

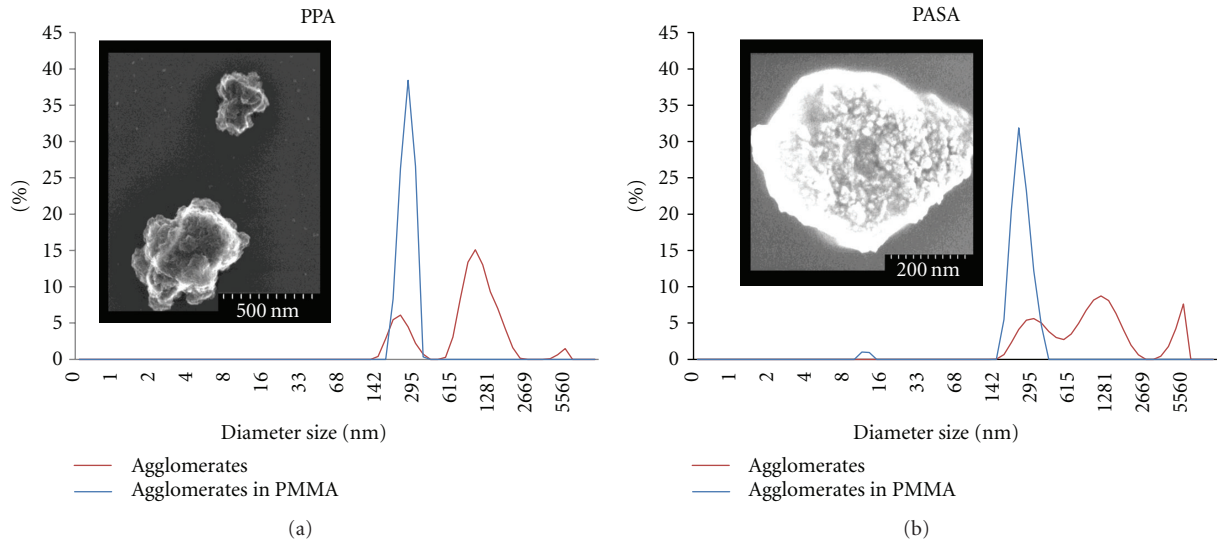


Figure 6: PA : $Tb^{3+}$ : $LaF_3$ (a) and ASA : $Tb^{3+}$ : $LaF_3$ (b) agglomerate diameters in water (red) and dispersed in PMMA/THF (blue) at 5 : 1 ligand to nanoparticle ratio. STEM images (inset) show representative agglomerates found in the polymer nanocomposite.

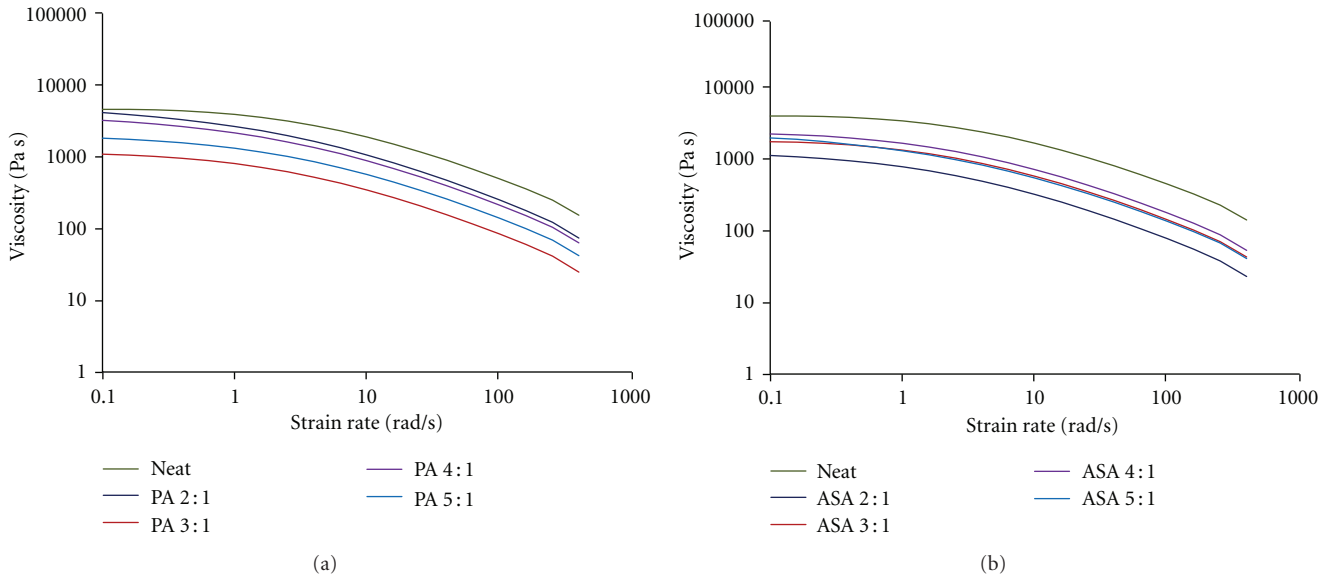


Figure 7: Complex viscosity as a function of frequency at 220°C for neat PMMA and PMMA nanocomposites of PA : $Tb^{3+}$ : $LaF_3$ (a) and ASA : $Tb^{3+}$ : $LaF_3$ (b) at varying ligand to nanoparticle ratios.

ASA : $Tb^{3+}$ : $LaF_3$ at the 5 : 1 ligand to nanoparticle ratio with STEM images in the inset are illustrated in Figures 6 (a) and 6 (b), respectively.

Viscosity measurements were made by evaluating the relationship between complex viscosity and frequency. The relationship of complex viscosity to frequency is representative of the shear viscosity versus shear rate based on the Cox-Merz rule which states that the magnitudes of complex and shear viscosity data can be compared at equal values of frequency and shear rate [18]. Figure 7 shows the measured complex viscosity with varying frequency for neat PMMA and the nanocomposite PMMA with ligand to nanoparticle ratios of 2 : 1, 3 : 1, 4 : 1, and 5 : 1. All of the samples exhibited a traditional shear thinning behavior where Newtonian fluid behavior occurred at low frequencies and shear thinning behavior occurring at higher frequencies in a similar manner to the nanoparticle loading samples. The incorporation of nanoparticles caused a reduction in the viscosity of the composites for all the ratios studied as seen in Figure 7. The calculated values of percent difference in the average complex viscosity at 10 rad/s between the neat PMMA and nanocomposite PMMA are displayed in Table 3. In the case of PA capped nanoparticles, the reduction in average agglomerate size (from ~450 nm to 150 nm) corresponded with the lower values for the measured complex viscosity values (44% to 82% reduction in complex viscosity), in that the lower the

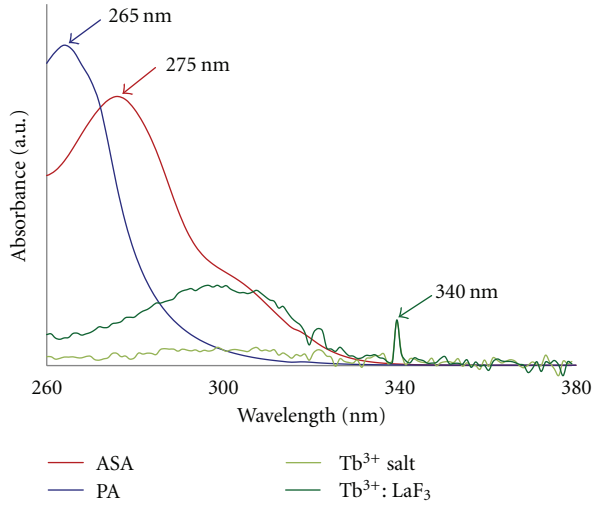


FIGURE 8: Absoption spectra of PA (blue), ASA (red) ligand, $Tb^{3+}$ salt (light green), and $Tb^{3+}:LaF_3$ (dark green) in water.

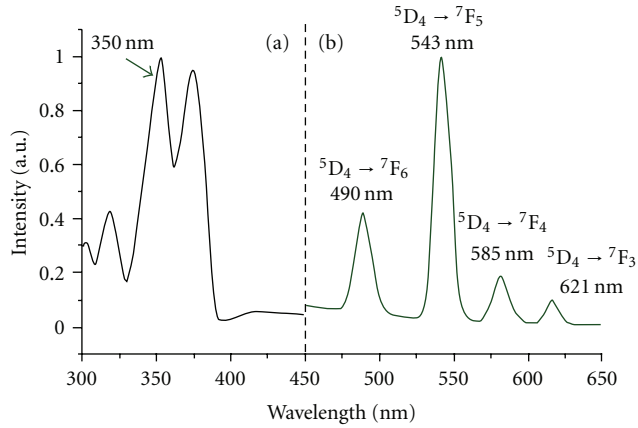


FIGURE 9: Characteristic (a) excitation spectrum ($\lambda_{em}$ = 542 nm) and (b) emission peaks of $Tb^{3+}:LaF_3$ ($\lambda_{ex}$ = 375 nm) [23].

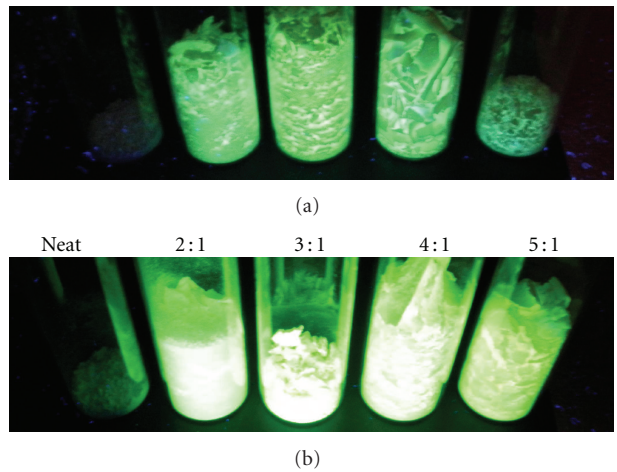


FIGURE 10: Neat PMMA and PMMA nanocomposites composed of varying ratios of (a) $PA:Tb^{3+}:LaF_3$ and (b) $ASA:Tb^{3+}:LaF_3$ under UV light.

agglomerate size the lower the viscosity observed. This trend was not seen in the case of the ASA system.

Overall, the lower viscosity values could be the result of the nanoparticles acting to break up the structure interfering with the local intermolecular hydrogen bonding, and enabling polymer chains to slip past the nanoparticles resulting in less resistance [19]. An alternative hypothesis might also be attributed to a small decrease of polymer molecular entanglement density as a function of the high aspect ratio of the nanoparticles causing disruption in the polymer chain entangled network [20], allowing the chains to slip past one another hence lowering the viscosity. Therefore, it is fair to extrapolate that the particles act as transient lubricants which may lead to a lower processing temperature profile for melt extrusion [21, 22].

Figure 8 shows the UV-Vis spectra for the PA ligand (blue), ASA ligand (red), $Tb^{3+}$ salt, that is, $Tb(NO_3)_3 \cdot 6H_2O$, (light green) and $Tb^{3+}:LaF_3$ (dark green) in water. The peak value for the PA ligand was measured at 265 nm and for the ASA ligand was 275 nm. These values were used as the ligand excitation wavelength to evaluate the energy transfer of the ligand to the RE ion. The peak value for the $Tb^{3+}$ salt and $Tb^{3+}:LaF_3$, respectively, was measured at 340 nm.

Figure 9 (a) is the excitation spectrum of $Tb^{3+}:LaF_3$ which demonstrates the presence of peaks within the UV region that are representative of $^7F_6 \rightarrow {}^5D_3$, $^7F_6 \rightarrow {}^5G_J$, and $^7F_6 \rightarrow {}^5L_6$ ground state absorptions of the$Tb^{3+}$ ion [23]. The characteristic $Tb^{3+}$ emission peaks that occur within the visible region at 490, 543, 585, and 621 nm coincide with $^5D_4 \rightarrow {}^7F_6$, $^5D_4 \rightarrow {}^7F_5$, $^5D_4 \rightarrow {}^7F_4$, and $^5D_4 \rightarrow {}^7F_3$ transitions, respectively and are shown in Figure 9 (b). The most intense emission band was observed at 543 nm where green light is emitted. The luminescence of the various ratios of ligand to rare-earth PMMA nanocomposites when excited with UV light at the wavelength of 365 nm is visually apparent from the images in Figure 10.

Upon excitation of the $Tb^{3+}$ absorption band at 350 nm ($\lambda_{ex}$), the emission spectrum generates the characteristic emission peaks found in Figure 9 (b). When the UV light harvesting organic ligand is excited the emission is effectively sensitized due to the energy transfer to the RE ion [24]. In the case where the ligand is excited the characteristic emission spectra peaks of the ion would exist if energy transfer to $Tb^{3+}$ is successful. Analysis of the UV-Vis spectra (Figure 8) suggests that the excitation wavelength for PA is 265 nm and ASA is 275 nm hence both nanocomposites exhibited the characteristic $Tb^{3+}$ emission peaks.

Sharp emission spectra (FWHM < 5 nm) are generally preferred than broad emission spectra (FWHM = 50–200 nm) which organic dyes typically produce for photonic devices [25]. Sharp or narrow emission peaks are preferred as a result of improving color saturation where saturation is the perceived intensity relative to its own brightness [26]. In order to characterize the photoluminescence of the optical polymer nanocomposites the spectra were normalized at the characteristic peak of 543 nm and Lorentzian fits were applied. The FWHM at the 490 nm emission peaks was measured. The 490 nm peak of $Tb^{3+}$ is considered to occur as

Table 4: FWHM values for PMMA nanocomposites composed of varying ratios of PA : $Tb^{3+}$ : $LaF_3$.

| Ligand | Ligand to nanoparticle ratio | FWHM of 490 nm peak—direct ion excitation ($\lambda_{ex}$= 350 nm) | FWHM of 490 nm peak—ligand excitation ($\lambda_{ex}$ = 265 nm) |
|---|---|---|---|
| PA | 2 : 1 | 9.64 ± 0.36 nm | 8.51 ± 0.20 nm |
| | 3 : 1 | 9.01 ± 0.19 nm | 8.53 ± 0.18 nm |
| | 4 : 1 | 9.18 ± 0.34 nm | 8.50 ± 0.20 nm |
| | 5 : 1 | 9.81 ± 0.39 nm | 8.95 ± 0.20 nm |

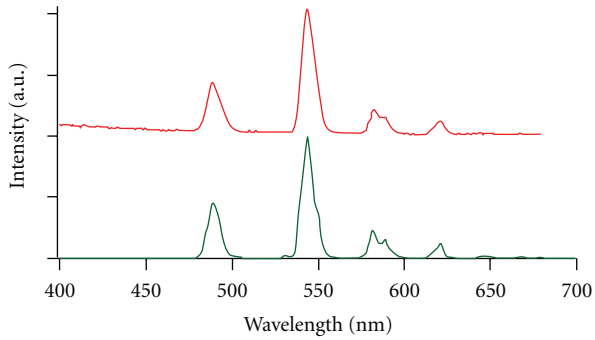


Figure 11: Emission of $Tb^{3+}$ doped $LaF_3$ in PMMA nanocomposites composed of 2 : 1 PA ligand to ion ratio at two different excitation wavelengths (red-$\lambda_{ex}$ = 350 nm and green-$\lambda_{ex}$ = 265 nm) The spectra are normalized to the 540 nm peak.

the result of an electric dipole transition which by nature is affected by changes in the environment [27]. The ASA system under direct ion or ligand excitation produced FWHM values ≈11 nm regardless of ligand to ion ratio. The PA system produced FWHM values from ligand excitation that were lower than values produced by direct ion excitation as shown in Table 4. Representative emission spectra of PMMA PA : $Tb^{3+}$ : $LaF_3$ nanocomposite excited at 350 nm (direct ion excitation—red) and 265 nm (ligand excitation—green) are shown in Figure 11.

## 4. Conclusions

Light-emitting polymer nanocomposites were produced via solution/precipitation chemistry using ligand capped nanocrystals doped with $Tb^{3+}$ ions loaded into PMMA. The incorporation of ligand (ASA and PA) : $Tb^{3+}$ : $LaF_3$ nanoparticles within the PMMA matrix was verified by ATR-FTIR spectroscopy (organic) and TGA (inorganic). The absorbance spectrum obtained from ATR-FTIR spectroscopy of the ASA system produced absorption peaks at 1601 $cm^{-1}$ and 1559 $cm^{-1}$ which corresponds with benzene ring stretching. The PA : $Tb^{3+}$ : $LaF_3$ absorbance spectrum exhibited absorption peaks at 1653 $cm^{-1}$, 1593 $cm^{-1}$, and 1568 $cm^{-1}$ which suggest that the pyridine ring of picolinic acid is stretching. The peak located at ~1341 $cm^{-1}$ could be associated with C-N stretching vibrations of the PA ligand.

Thermogravimetric analysis of PMMA nanocomposites showed that the ASA : $Tb^{3+}$ : $LaF_3$ contained system ~10 wt% inorganic material, whereas the PA : $Tb^{3+}$ : $LaF_3$ system contained approximately 7 wt% inorganic material. The EDS analysis confirmed that PA : $Tb^{3+}$ : $LaF_3$ was on average at a 6 : 1 molar ratio of $La^{3+}$ to $Tb^{3+}$ and ASA : $Tb^{3+}$ : $LaF_3$ was on average at a 4 : 1 molar ratio of La to $Tb^{3+}$.

The average diameter for PA : $Tb^{3+}$ : $LaF_3$ and ASA : $Tb^{3+}$ : $LaF_3$ at varying ligand to nanoparticle ratios produced agglomerates with diameters > 200 nm in PMMA. The resuspension liquid (water or THF) showed no significant difference in agglomerate size for PMMA nanocomposites of PA : $Tb^{3+}$ : $LaF_3$ and ASA : $Tb^{3+}$ : $LaF_3$ at ligand : nanoparticle ratios of 2 : 1, 3 : 1, and 4 : 1. However, a significant particle size difference was observed at the 5 : 1 ratio where those resuspended in water were measured at 893 ± 418 nm and 1080 ± 192 nm for ASA and PA systems, respectively. For the same ratio resuspended in THF values were measured at 233 ± 41 nm for ASA and 242 ± 24 nm for PA.

The rheology measurements for all samples produced traditional shear thinning curves. The addition of the agglomerates caused a reduction in the viscosity of all PMMA nanocomposites as compared to neat PMMA. The PA : $Tb^{3+}$ : $LaF_3$ PMMA nanocomposites exhibited a reduction in viscosity that corresponded with the reduction in the size of the agglomerates. The ASA nanocomposite demonstrated lower viscosity values but did not exhibit the same trend with respect to agglomerate size.

Green light was produced by direct ion and ligand excitation of ASA and PA PMMA nanocomposite. All emission spectra exhibited the corresponding characteristic emission of trivalent terbium.

## Acknowledgments

The authors acknowledge the support and fellowship funding at the time of this work provided by the South East Alliance for Graduate Education and the Professoriate (SEAGEP) on the National Science Foundation Award HRD-0450279, Center of Optical Materials Science and Engineering Technologies (COMSET), and School of Materials Science and Engineering at Clemson University. A note of gratitude is given to Dr. Gregory Von White II, Courtney Kucera, and Kim Ivey for their help with this paper.

## References

[1] Z. L. Wang, Z. W. Quan, P. Y. Jia et al., "A facile synthesis and photoluminescent properties of redispersible $CeF_3$, $CeF_3$:$Tb^{3+}$, and $CeF_3$:$Tb^{3+}$/$LaF_3$ (core/shell) nanoparticles," *Chemistry of Materials*, vol. 18, no. 8, pp. 2030–2037, 2006.

[2] P. K. Sharma, R. Nass, and H. Schmidt, "Effect of solvent, host precursor, dopant concentration and crystallite size on the fluorescence properties of Eu(III) doped yttria," *Optical Materials*, vol. 10, no. 2, pp. 161–169, 1998.

[3] V. Bekiari and P. Lianos, "Multicolor emission from terpyridine-lanthanide ion complexes encapsulated in nanocomposite silica/poly(ethylene glycol) sol-gel matrices," *Journal of Luminescence*, vol. 101, no. 1-2, pp. 135–140, 2003.

[4] E. Brunet, O. Juanes, and J. Rodriguez-Ubis, "Supramolecularly organized lanthanide complexes for efficient metal excitation and luminescence as sensors in organic and biological

applications," *Current Chemical Biology*, vol. 1, no. 1, pp. 11–39, 2007.

[5] H. Jiu, L. Zhang, G. Liu, and T. Fan, "Fluorescence enhancement of samarium complex co-doped with terbium complex in a poly(methyl methacrylate) matrix," *Journal of Luminescence*, vol. 129, no. 3, pp. 317–319, 2009.

[6] R. R. Tang, G. L. Gu, and Q. Zhao, "Synthesis of Eu(III) and Tb(III) complexes with novel pyridine dicarboxamide derivatives and their luminescence properties," *Spectrochimica Acta—Part A*, vol. 71, no. 2, pp. 371–376, 2008.

[7] Z. Wang, M. Li, C. Wang, J. Chang, H. Shi, and J. Lin, "Photoluminescence properties of $LaF_3$: $Eu^{3+}$ nanoparticles prepared by refluxing method," *Journal of Rare Earths*, vol. 27, no. 1, pp. 33–37, 2009.

[8] L. G. Jacobsohn, K. B. Sprinkle, C. J. Kucera et al., "Synthesis, luminescence and scintillation of rare earth doped lanthanum fluoride nanoparticles," *Optical Materials*, vol. 33, no. 2, pp. 136–140, 2010.

[9] B. Kokuoz, J. R. DiMaio, C. J. Kucera, D. D. Evanoff, and J. Ballato, "Color kinetic nanoparticles," *Journal of the American Chemical Society*, vol. 130, no. 37, pp. 12222–12223, 2008.

[10] B. Kokuoz, C. Kucera, J. R. DiMaio, and J. Ballato, "Organic—inorganic hybrid nanoparticles with enhanced rare-earth emissions," *Optical Materials*, vol. 31, no. 9, pp. 1327–1330, 2009.

[11] Y. Luo, X. Yu, W. Su et al., "Energy transfer in a ternary system composed of $Tb(DBM)_3Phen$, $Eu(DBM)_3Phen$, and poly(N-vinylcarbazole)," *Journal of Materials Research*, vol. 24, no. 10, pp. 3023–3031, 2009.

[12] S. Maji and K. S. Viswanathan, "Ligand-sensitized fluorescence of $Eu^{3+}$ using naphthalene carboxylic acids as ligands," *Journal of Luminescence*, vol. 128, no. 8, pp. 1255–1261, 2008.

[13] I. G. Binev, B. A. Stamboliyska, and Y. I. Binev, "The infrared spectra and structure of acetylsalicylic acid (aspirin) and its oxyanion: an ab initio force field treatment," *Journal of Molecular Structure*, vol. 378, no. 3, pp. 189–197, 1996.

[14] L. C. Thompson, "Complexes of the rare earths. VIII. Picolinic acid," *Inorganic Chemistry*, vol. 3, no. 9, pp. 1319–1321, 1964.

[15] R. Dangtungee, J. Yun, and P. Supaphol, "Melt rheology and extrudate swell of calcium carbonate nanoparticle-filled isotactic polypropylene," *Polymer Testing*, vol. 24, no. 1, pp. 2–11, 2005.

[16] B. M. Ellerbrook, *Fabrication of fluorescent nanoparticle-polymer compoites for photoactive-based materials*, M.S. thesis, 2010.

[17] L. Ravina, *Everything You Want to Know about Coagulation & Flocculation*, Zeta-Meter, Staunton, Va, USA, 4th edition, 1993.

[18] R. Bird, R. Armstrong, and O. Hassager, Eds., *Dynamics of Polymeric Liquids, Volume 1, Fluid Mechanics*, vol. 1, John Wiley & Sons, New York, NY, USA, 1977.

[19] H. Barnes, *A Handbook of Elementary Rheology*, vol. 1, The University of Wales Institute of Non-Newtonian Fluid Mechanics, Wales, UK, 2000.

[20] S. G. Hatzikiriakos, N. Rathod, and E. B. Muliawan, "The effect of nanoclays on the processibility of polyolefins," *Polymer Engineering and Science*, vol. 45, no. 8, pp. 1098–1107, 2005.

[21] H. E. Sliney, "Rare-earth fluorides and oxides—an exploratory study of their use as solid lubricants at temperatures to 1800°F (1000°C)," 1–26.

[22] Z. Zhang, L. Yu, W. Liu, and Q. Xue, "Effect of $LaF_3$ nanocluster modified with succinimide on the lubricating performance of liquid paraffin for steel-on-steel system," *Tribology International*, vol. 34, no. 2, pp. 83–88, 2001.

[23] J. Wang, S. Bo, L. Song, J. Hu, X. Liu, and Z. Zhen, "One-step synthesis of highly water-soluble $LaF_3$:$Ln^{3+}$ nanocrystals in methanol without using any ligands," *Nanotechnology*, vol. 18, no. 46, article 465606, 2007.

[24] J. Mezyk, D. Di Nuzzo, A. Mech, R. Tubino, and F. Meinardi, "Exciton-exciton annihilation in organic lanthanide complexes," *Journal of Chemical Physics*, vol. 132, article 024504, 2010.

[25] M. A. Diaz-Garcia, S. F. De Avila, and M. G. Kuzyk, "Energy transfer from organics to rare-earth complexes," *Applied Physics Letters*, vol. 81, no. 21, pp. 3924–3926, 2002.

[26] M. D. Fairchild, "In color appearance models: CIECAM02 and beyond," in *Proceedings of the IS&T/SID 12th Color Imaging Conference*, pp. 1–68, Scottsdale, Ariz, USA, November 2004.

[27] P. R. Selvin and J. E. Hearst, "Luminescence energy transfer using a terbium chelate: improvements on fluorescence energy transfer," *Proceedings of the National Academy of Sciences of the United States of America*, vol. 91, no. 21, pp. 10024–10028, 1994.